

**Noise Error Budget for Quantum Error Correction using
Gottesmann-Kitaev-Preskill States in Trapped Ions**

by

Arne Jakob Geipel

A

Semester Project

in the

MSc Physics at ETH Zürich

conducted in the

Trapped Ion Quantum Information Group

Zurich, Switzerland

July 9, 2024

Supervised by: Moritz Fontboté-Schmidt, Florence Berterottière, and Dr. Stephan Welte
in the research group of Prof. Dr. Jonathan Home

Abstract

Bosonic codes, like the Gottesman-Kitaev-Preskill (GKP) code, are promising candidates for quantum information processing with low overhead for quantum error correction. Stabilization of GKP codewords has been demonstrated experimentally in trapped ions and superconducting circuits. In the latter, break-even with the best physical encoding of the system has been recently achieved with a gain factor of 2.3. Here, a simple noise model is developed, which aims to describe the decoherence of a stabilized GKP state generated in the motional degree of freedom of a trapped ion. This model assumes the stabilization circuit to be instantaneous and noise-free, which leaves room for future improvement of the model to accurately predict experimental results. Using this simplified noise model simulations are carried out, which indicate that error correction improves the lifetime of a GKP state from 0.48(2) ms to 1.45(5) ms. The model is further employed to study how the coherence time depends on the GKP state size. Finally, the noise error budget of the error correction protocol is computed, analyzing how improvements in the respective error rates of the noise model would translate to a lifetime improvement of the GKP state. The simulations indicate dephasing as the dominant noise source with 80 % contribution in the current state of the experiment. Direct experimental conclusions are difficult because of the simplifications made in the noise model. However, the presented methods for extracting metrics for error correction from a given noise model can also be applied to more general cases in the future.

Contents

Title Page	i
Abstract	ii
Table of Contents	iii
Acknowledgements	iv
1 Introduction	1
2 Square-Lattice GKP Code	3
3 Stabilization of Finite Energy GKP States	7
4 Oscillator Noise Model	11
5 Noise Error Budget Simulation	16
6 Conclusion and Outlook	19
Bibliography	21

Acknowledgements

I would like to thank Moritz Fontboté-Schmidt, Florence Berterottière, and Stephan Welte, the GKP TIQI's, for many stimulating discussions and for providing me with the opportunity to carry out my semester project with the GKP team. I am grateful to Ivan Rojkov and Elias Zapusek for insightful theoretical discussions on bosonic codes. I would also like to thank my fellow semester project students, Luise Müller and Foivos Vouzinas, for helpful discussions and for an enjoyable time in the group office. For their insightful suggestions regarding the semester project during the group meetings, I would like to thank Jonathan Home and Daniel Kienzler. Additionally, I would like to thank Jonathan Home for the opportunity to conduct my semester project in the TIQI Group. Finally, I thank the entire TIQI group for making this semester project, including the TIQI skiing retreat, a very pleasurable experience.

1 Introduction

Operation of useful [1] large-scale quantum algorithms crucially requires high-quality gates paired with a qubit coherence time that sufficiently exceeds the gate time. [2, 3] Stabilizer codes [4, 5] introduce redundancy into the qubit encoding, which allows scaling of the qubit coherence time using quantum error correction (QEC) given sufficiently good operations. [6–10] Error correction paves the way towards a fault-tolerant universal set of gates [11] and, ultimately, operation of increasingly large quantum algorithms [2, 12].

Prominent examples of error correction codes include the surface code [13] and the color code [14], which encode a logical qubit into multiple physical qubits. It has been shown experimentally that a 49-qubit distance 5 ($d = 5$) surface code outperforms a 17-qubit distance 3 ($d = 3$) surface code in terms of logical error rates. [7] Although this work by Google Quantum AI demonstrates how the lifetime of a logical qubit can be improved, it also reveals one of the key difficulties in scaling the surface or color code: physical qubit overhead. Reducing the overall qubit resources required for logical operations is a central topic of ongoing research efforts. [15–18]

Bosonic error correction codes like the Gottesmann-Kitaev-Preskill (GKP) code [19] achieve encoding of a logical qubit into a harmonic oscillator in a way that naturally allows for stabilization of the logical code space with a single harmonic oscillator system, i.e., with no physical qubit overhead. [19, 20] Encoding a qubit in a GKP state has been first demonstrated in the motional degree of freedom of a trapped ion [21, 22]. Stabilization of the GKP code space has been realized experimentally in superconducting circuits [9] and trapped ions [8], with superconducting circuits recently achieving break-even with a gain factor of 2.3 with the best physical encoding of the system. [10] Recent proposals on how to realize two-qubit gates [23] and non-Clifford gates [24, 25] on finite-energy GKP codes render the GKP code a promising candidate for quantum information processing. Furthermore, encoding a qubit in a GKP state turns out to also be favorable for enhanced quantum transduction [26], potentially allowing for distributed quantum computation with superconducting circuits in the future.

This semester project report reviews the GKP code (ch. 2) and its stabilization (ch. 3) in order to then introduce a simple oscillator noise model (ch. 4) that aims to describe the error sources contributing towards the decoherence of a stabilized GKP state realized in the motional degree

1 Introduction

of freedom of a trapped ion. This model assumes the stabilization circuit to be instantaneous and noise-free, which leaves room for future improvement of the model to accurately predict experimental results. The simplified noise model is employed to simulate the time evolution of an error-corrected GKP state. These simulations, e.g., allow for the prediction of the logical lifetime improvement due to stabilization. Furthermore, given the noise model, a method is introduced to compute the noise error budget (ch. 5). The computed error budget suggests dephasing as the dominant error source in the system. However, drawing direct conclusions for the experiment turns out to be difficult because of the simplifications made in the noise model. Finally, the quality of the noise model is evaluated critically with regard to its capability to predict the coherence time of a Fock state (ch. 6).

2 Square-Lattice GKP Code

The GKP code space is defined as a subspace of the Hilbert space \mathcal{H}_{HO} of a harmonic oscillator. [19, 26, 27] We start from a harmonic oscillator with dimensionless position and momentum quadrature operators $\hat{x} = (\hat{a} + \hat{a}^\dagger)/\sqrt{2}$ and $\hat{p} = i(\hat{a}^\dagger - \hat{a})/\sqrt{2}$, where \hat{a} and \hat{a}^\dagger are the bosonic creation and annihilation operators which fulfill the commutation relation $[\hat{a}, \hat{a}^\dagger] = 1$. We follow the convention $\hbar = 1$ such that $[\hat{x}, \hat{p}] = i$. Given a harmonic oscillator system, we can define the two stabilizers for the ideal GKP code [20, 26]

$$\hat{T}_{x,0} = e^{i2\sqrt{\pi}\hat{x}} \quad (2.1)$$

$$\hat{T}_{p,0} = e^{-i2\sqrt{\pi}\hat{p}}. \quad (2.2)$$

These operators displace a given state by $2\sqrt{\pi}$ in phase space along the x (p) quadrature for $\hat{T}_{p,0}$ ($\hat{T}_{x,0}$), respectively. Note, how the choice of the magnitude $2\sqrt{\pi}$ of the displacement implies¹ $[\hat{T}_{x,0}, \hat{T}_{p,0}] = 0$, i.e., we can find states that are invariant under displacements along both quadratures simultaneously. We define the GKP code space \mathcal{C} to precisely contain these states [26]

$$\mathcal{C} = \left\{ |\psi\rangle : \hat{T}_{x,0} |\psi\rangle = \hat{T}_{p,0} |\psi\rangle = +1 |\psi\rangle \right\}. \quad (2.3)$$

This code space is the result of the specific choice $S = \mathbb{1}_{2 \times 2}$ and $d = 2$ for the symplectic matrix S and integer value d defined in [26] and known as the two-dimensional square-lattice GKP code. The Pauli operators for this code are given by [20, 26]

$$\hat{Z}_0 = \sqrt{\hat{T}_{x,0}} = \sqrt{e^{i2\sqrt{\pi}\hat{x}}} = e^{i\sqrt{\pi}\hat{x}} \quad (2.4)$$

$$\hat{X}_0 = \sqrt{\hat{T}_{p,0}} = \sqrt{e^{-i2\sqrt{\pi}\hat{p}}} = e^{-i\sqrt{\pi}\hat{p}}. \quad (2.5)$$

¹Following the discussion in [26], a displacement in phase space by $\mathbf{u} = (u_x, u_p)^T$ is generated by the operator $\hat{T}(\mathbf{u}) \equiv \exp[i(u_p \hat{x} - u_x \hat{p})]$. Furthermore, $\hat{T}(\mathbf{u})\hat{T}(\mathbf{v}) = e^{-i\omega(\mathbf{u}, \mathbf{v})}\hat{T}(\mathbf{v})\hat{T}(\mathbf{u})$ with $\omega(\mathbf{u}, \mathbf{v}) = \det \begin{pmatrix} \mathbf{u}^T \\ \mathbf{v}^T \end{pmatrix}$. Consequently, the phase $\omega(\mathbf{u}, \mathbf{v})$ can be interpreted geometrically as the oriented area of the parallelogram spanned by the displacement vectors \mathbf{u} and \mathbf{v} . Commuting displacement operators, therefore, require this parallelogram to have an area $2\pi d$ with d an integer value.

2 Square-Lattice GKP Code

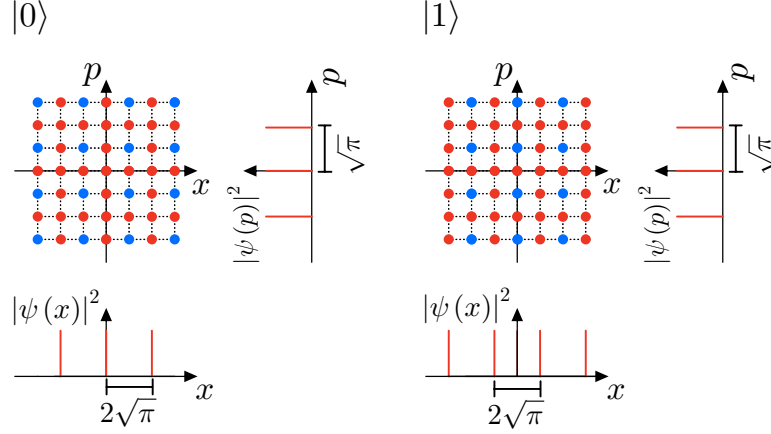


Figure 2.1: Phase space representations and probability densities in x and p basis of ideal square-lattice GKP states $|0\rangle$ and $|1\rangle$. Red (blue) points indicate a positive (negative) value of the Wigner function. One should imagine the Wigner functions with an infinite extent. Note how the Wigner functions are invariant under a displacement of magnitude $2\sqrt{\pi}$ along the x and p quadrature. This implies that the states lie in the code space \mathcal{C} . Furthermore, note how the Wigner functions of the $|0\rangle$ and $|1\rangle$ state are related by a displacement of $\sqrt{\pi}$ along the x quadrature, which corresponds to applying the Pauli \hat{X}_0 operator. Similar considerations can be made for applying the Pauli \hat{Z}_0 and \hat{Y}_0 operators as well as for their respective eigenstates.

It is straightforward to check that these operators fulfill the required commutation relation $\hat{X}_0\hat{Z}_0 = -\hat{Z}_0\hat{X}_0$. The remaining Pauli operator \hat{Y}_0 can be constructed from \hat{X}_0 and \hat{Z}_0 and is given by $\hat{Y}_0 = -i\hat{Z}_0\hat{X}_0$. [20] Therefore, also the logical operators of the GKP code correspond to displacements in phase space. Overall, this code achieves a subspace decomposition of the continuous variable Hilbert space of a harmonic oscillator into a discrete-variable Hilbert space $\mathcal{C} \simeq \mathbb{C}^2$ that serves as the logical subspace and a remaining "wilderness space" $\mathcal{H}_{\text{wild}} = \mathcal{H}_{\text{HO}} \setminus \mathcal{C}$ such that $\mathcal{H}_{\text{HO}} = \mathcal{C} \oplus \mathcal{H}_{\text{wild}}$. [27]

We choose the eigenstates $|\mu_0\rangle$ of the \hat{Z}_0 operator with $\mu \in \{0, 1\}$ as the basis states of the GKP code space \mathcal{C} [26], with

$$\hat{Z}_0 |0\rangle = +1 |0\rangle \quad (2.6)$$

$$\hat{Z}_0 |1\rangle = -1 |1\rangle. \quad (2.7)$$

In the x -quadrature eigenbasis, the logical states $|0\rangle$ and $|1\rangle$ are given by Dirac combs [20,26]

$$|0\rangle \propto \sum_{k \in \mathbb{Z}} |x = 2\sqrt{\pi}k\rangle \quad (2.8)$$

$$|1\rangle \propto \sum_{k \in \mathbb{Z}} |x = 2\sqrt{\pi}(k + 1/2)\rangle. \quad (2.9)$$

2 Square-Lattice GKP Code

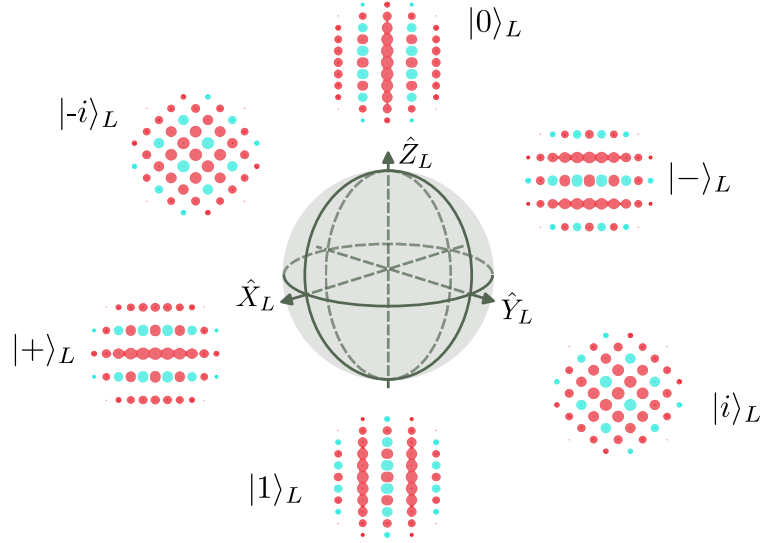


Figure 2.2: Bloch sphere of the finite energy square-lattice GKP code. Phase space representations of the eigenstates of the finite energy Pauli operators are shown. In the context of this report, the eigenstates of the finite energy Pauli operators of the GKP code are referred to with an index L . Figure obtained from Ivan Rojko with kind permission.

Figure 2.1 shows a schematic plot of the phase space representations of the $|0_0\rangle$ and $|1_0\rangle$ state, respectively.

The ideal GKP states introduced above are not normalizable and, therefore, unphysical. In order to describe physical GKP states, one can introduce an envelope operator $\hat{E}_\Delta = \exp(-\Delta^2 \hat{a}^\dagger \hat{a})$ to limit the energy contained in a GKP state to a finite value. The finite energy GKP states are then defined by

$$|0_\Delta\rangle = \mathcal{N}_\Delta^0 \hat{E}_\Delta |0_0\rangle \quad (2.10)$$

$$|1_\Delta\rangle = \mathcal{N}_\Delta^1 \hat{E}_\Delta |1_0\rangle \quad (2.11)$$

with normalization factors \mathcal{N}_Δ^0 and \mathcal{N}_Δ^1 . [20] The envelope operator modulates the infinite energy GKP states with a Gaussian envelope whose width is defined by the parameter Δ . [9] For $\Delta = 0$, the infinite energy GKP states $|0_0\rangle$ and $|1_0\rangle$ are recovered. Both the stabilizers and Pauli operators for the finite energy GKP code can be defined by applying the envelope operator \hat{E}_Δ [20]

$$\hat{\bullet}_0 \rightarrow \hat{\bullet}_\Delta \equiv \hat{E}_\Delta \hat{\bullet}_0 \hat{E}_\Delta^{-1}, \quad (2.12)$$

2 Square-Lattice GKP Code

where $\hat{\bullet}_0$ denotes an ideal GKP code stabilizer or Pauli operator and $\hat{\bullet}_\Delta$ the corresponding finite energy counterpart. The finite energy square-lattice GKP code space \mathcal{C}_Δ is then defined by

$$\mathcal{C}_\Delta = \left\{ |\psi\rangle : \hat{T}_{x,\Delta} |\psi\rangle = \hat{T}_{p,\Delta} |\psi\rangle = +1 |\psi\rangle \right\}. \quad (2.13)$$

Figure 2.2 shows the Wigner functions of the eigenstates of the finite energy Pauli operators \hat{X}_Δ , \hat{Y}_Δ , and \hat{Z}_Δ , respectively. A discussion of the finite energy stabilizers, Pauli operators, and GKP states is carried out in [20].

3 Stabilization of Finite Energy GKP States

As with any quantum system, the harmonic oscillator utilized to store a GKP state described in chapter 2 will couple to the environment. This gives rise to various noise channels, which in turn lead to decoherence of the quantum state. [28] The noise channels dominant in the GKP setup at TIQI group are discussed in chapter 4. Increasing the lifetime of information encoded in GKP states, therefore, requires a mechanism to stabilize the code space \mathcal{C}_Δ .

Starting from the finite energy stabilizers $\hat{T}_{x,\Delta}$ and $\hat{T}_{p,\Delta}$, operators $\hat{d}_{x,\Delta}$ and $\hat{d}_{p,\Delta}$ can be constructed [20] such that

$$\hat{T}_{x,\Delta} |\psi\rangle = +1 |\psi\rangle \Leftrightarrow \hat{d}_{x,\Delta} |\psi\rangle = 0 \quad (3.1)$$

$$\hat{T}_{p,\Delta} |\psi\rangle = +1 |\psi\rangle \Leftrightarrow \hat{d}_{p,\Delta} |\psi\rangle = 0. \quad (3.2)$$

In order to force an arbitrary initial state into the logical subspace \mathcal{C}_Δ , it is sufficient to engineer an oscillator-bath interaction that realizes the dissipators $\mathcal{D}[\hat{d}_{x,\Delta}](\rho)$ and $\mathcal{D}[\hat{d}_{p,\Delta}](\rho)$ [20] such that the master equation governing the time evolution of the system reads

$$\dot{\rho} = \Gamma_x \mathcal{D}[\hat{d}_{x,\Delta}](\rho) + \Gamma_p \mathcal{D}[\hat{d}_{p,\Delta}](\rho) \quad (3.3)$$

in the rotating frame, with $\mathcal{D}[\hat{L}](\rho) = \hat{L}\rho\hat{L}^\dagger - \frac{1}{2}\hat{L}^\dagger\hat{L}\rho - \frac{1}{2}\rho\hat{L}^\dagger\hat{L}$. Here, Γ_x and Γ_p are the damping rates¹ at which the operators $\hat{d}_{x,\Delta}$ and $\hat{d}_{p,\Delta}$ are applied to the state of the system. If the harmonic oscillator system is governed by the equation above, any initial state of the oscillator will asymptotically reach a steady state that is an element of the code space $\text{End}(\mathcal{C}_\Delta)$ ². In particular, the lifetime of a state that is an element of the code space \mathcal{C}_Δ will be prolonged.

It can be shown that the dissipators $\mathcal{D}[\hat{d}_{x,\Delta}](\rho)$ and $\mathcal{D}[\hat{d}_{p,\Delta}](\rho)$ can be approximately realized in a discretized fashion by applying phase space displacements conditioned on the state of an ancilla qubit $\{|g\rangle, |e\rangle\}$ initialized in the $|+\rangle = (|g\rangle + |e\rangle)/\sqrt{2}$ state³. [20] One discretized

¹Inspection of the unit of the master equation yields that Γ_\bullet is an angular frequency, i.e., $[\Gamma_\bullet] = \text{rad/s}$. Therefore, given a value $\#$ in the unit Hz, the value of the corresponding damping rate is given by $\Gamma_\bullet = 2\pi \times \#$ Hz. A value $\#$ given for a damping rate in the unit q/s (quanta per second) means $\Gamma_\bullet = \# \text{ rad/s} = \# \text{ q/s}$.

² $\text{End}(\mathcal{C}_\Delta)$ is the vector space of linear maps $\rho : \mathcal{C}_\Delta \rightarrow \mathcal{C}_\Delta$, i.e., of endomorphisms of \mathcal{C}_Δ .

³Note that preparing the ancilla in the $|+\rangle$ state is a choice specific to [20], which will be the main reference for this report. A slightly modified version of the stabilization protocol that requires initialization of the ancilla in the $|g\rangle$ state is described in [8]. Another approach, employing a feedback protocol to stabilize a GKP state in a superconducting microwave cavity, is described in [9].

3 Stabilization of Finite Energy GKP States

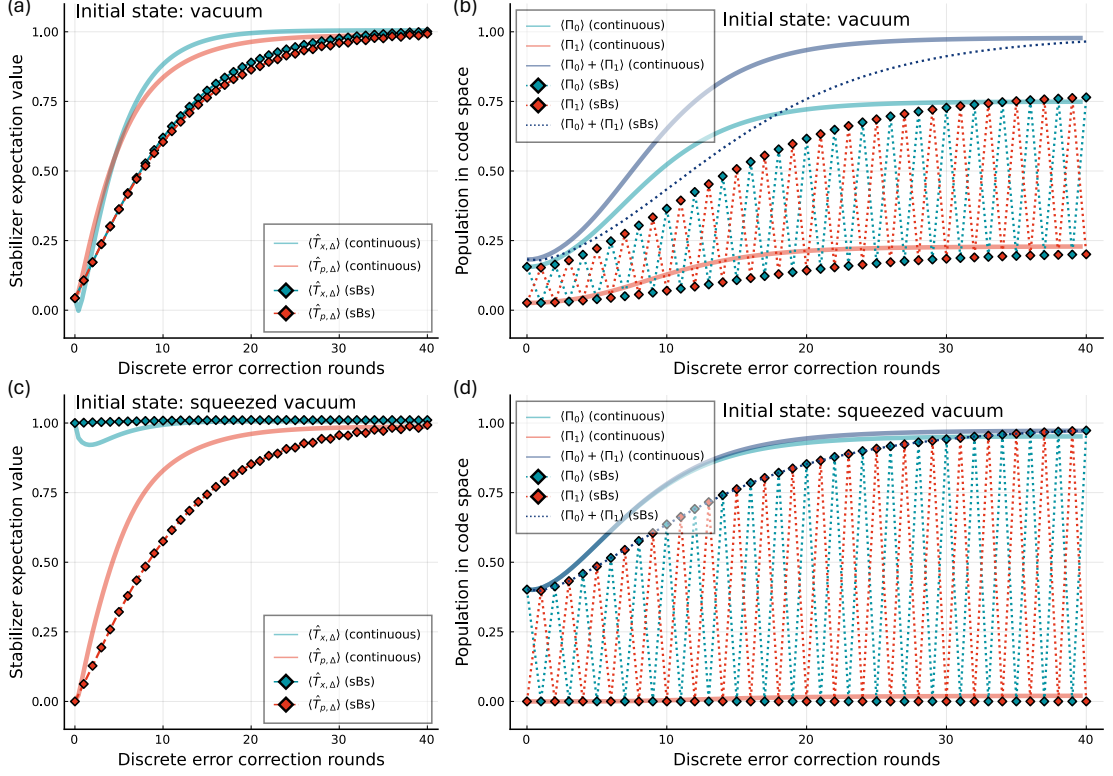


Figure 3.1: Stabilization of the finite energy GKP code space with $\Delta = 0.2$. GKP states are simulated for $x \in [-6\sqrt{\pi}, 6\sqrt{\pi}]$ with 150 discretization points. The chosen error correction rate is $\Gamma = \Gamma_x = \Gamma_p = 10$. Initial states are (a),(b) vacuum and (c),(d) squeezed vacuum with squeezing parameter $\xi = -\ln \sqrt{\tanh(\Delta^2)} \approx 1.6$ (for $\Delta = 0.2$) [20]. (a), (c) Finite energy stabilizer expectation value for continuous and sBs error correction protocol as a function of the number of discrete error correction rounds. Continuous and discrete stabilization are related via eq. 3.7. (b), (d) Population in logical GKP states $|0\rangle_L, |1\rangle_L$, and code space \mathcal{C}_Δ as a function of number of discrete error correction rounds. Projectors Π_0 and Π_1 are defined by $\Pi_0 = |0\rangle_L \langle 0|_L$ and $\Pi_1 = |1\rangle_L \langle 1|_L$.

stabilization cycle of both quadratures can be performed by applying the unitaries $\hat{U}_x^{(\text{sBs})}$ and $\hat{U}_p^{(\text{sBs})}$ successively to the system, where

$$\hat{U}_x^{(\text{sBs})} = \exp\left(\frac{-i\sqrt{\pi}s_\Delta}{2}\hat{p}\hat{\sigma}_y\right) \exp(-i\sqrt{\pi}c_\Delta\hat{x}\hat{\sigma}_x) \exp\left(\frac{-i\sqrt{\pi}s_\Delta}{2}\hat{p}\hat{\sigma}_y\right) \quad (3.4)$$

$$\hat{U}_p^{(\text{sBs})} = \exp\left(\frac{-i\sqrt{\pi}s_\Delta}{2}\hat{x}\hat{\sigma}_y\right) \exp(i\sqrt{\pi}c_\Delta\hat{p}\hat{\sigma}_x) \exp\left(\frac{-i\sqrt{\pi}s_\Delta}{2}\hat{x}\hat{\sigma}_y\right). \quad (3.5)$$

Here, $s_\Delta = \sinh \Delta^2$ and $c_\Delta = \cosh \Delta^2$. [20] The operators $\hat{\sigma}_x$ and $\hat{\sigma}_y$ correspond to the respective Pauli operators of the ancilla qubit. The state of the ancilla qubit has to be reset to the $|+\rangle$ state before applying the unitaries $U_x^{(\text{sBs})}$ and $U_p^{(\text{sBs})}$ such that one full error correction

3 Stabilization of Finite Energy GKP States

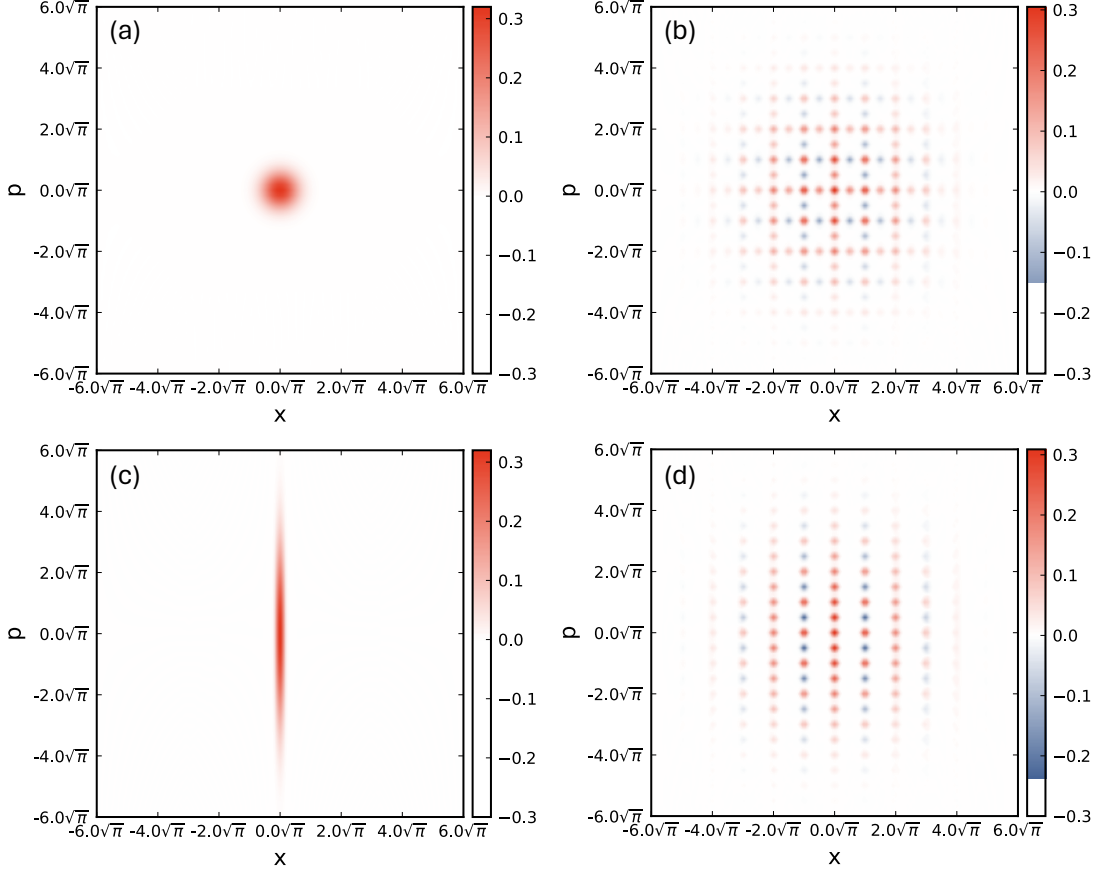


Figure 3.2: Wigner functions of initial and final states of the sBs protocol corresponding to figure 3.1. GKP states are simulated for $\Delta = 0.2$ and $x \in [-6\sqrt{\pi}, 6\sqrt{\pi}]$ with 150 discretization points. **(a)** Vacuum state. **(b)** Stabilized vacuum state after 40 sBs error correction rounds. Final state corresponds to partially mixed state with 0.784 purity. **(c)** Squeezed vacuum state with squeezing parameter $\xi = -\ln \sqrt{\tanh(\Delta^2)} \approx 1.6$ (for $\Delta = 0.2$) [20]. **(d)** Stabilized squeezed vacuum state after 40 sBs error correction rounds. Final state approximately corresponds to the state $|0\rangle_L$ with 97.3 % fidelity and 0.948 purity.

cycle $\rho_n \rightarrow \rho_{n+1}$ corresponds to applying the circuit

$$\rho_{n+1} = \text{Tr}_{\text{ancilla}} \left(\hat{U}_p^{(\text{sBs})} \left(\text{Tr}_{\text{ancilla}} \left(\hat{U}_x^{(\text{sBs})} (\rho_n \otimes |+\rangle \langle +|) \hat{U}_x^{(\text{sBs})\dagger} \right) \otimes |+\rangle \langle +| \right) \hat{U}_p^{(\text{sBs})\dagger} \right). \quad (3.6)$$

This discrete quantum error correction protocol is related to the continuous stabilization described by the master eq. 3.3 via the condition

$$\Gamma \delta t = \tanh(\Delta^2) (\sqrt{\pi} \cosh(\Delta^2))^2, \quad (3.7)$$

3 Stabilization of Finite Energy GKP States

assuming $\Gamma = \Gamma_x = \Gamma_p$. Given the duration $2 \times \delta t$ of the full stabilization cycle, i.e., of applying the circuit described in eq. 3.6, eq. 3.7 yields the corresponding error correction rate Γ for the continuous stabilization due to eq. 3.3. Eq. 3.7 results from approximating the continuous error correction protocol with a Trotter decomposition. [20]

The index "(sBs)" is short for "small-Big-small" and corresponds to the name of one of three approximate error correction protocols derived in [20]. The name refers to the relative magnitude of the applied conditional displacements. An optimized version of the sBs protocol is implemented in the GKP setup at TIQI group [8]. A discussion of the sBs error correction protocol and other possible approximate stabilization circuits is conducted in [20].

Figure 3.1 shows how the continuous and discretized error correction protocols stabilize the code space for a vacuum state and a squeezed vacuum state as initial states. The stabilizer expectation values and populations in the code space approach 1, which is testament to a successful stabilization of the GKP code (cf. figure 3.1 (a) and (c)). For vacuum as the initial state, the stabilization protocols yield a partially mixed state as the final state (cf. figure 3.1 (b)). For appropriately squeezed vacuum [20], the stabilization procedure approximately results in a pure state $|0\rangle_L$ ($|1\rangle_L$) for an even (odd) number of error correction rounds (cf. figure 3.1 (d)). Here, the $|0\rangle_L$ ($|1\rangle_L$) state is prepared with 97.3 % (97.1 %) fidelity and 0.948 (0.945) purity after 40 (39) discrete sBs error correction rounds. Note how the sBs protocol periodically flips the parity of the logical state. (cf. figure 3.1 (b) and (d) dotted lines) Because of that, the stabilization protocols can also be utilized for state preparation given an appropriate initial state.⁴ The Wigner functions of the initial and final states of the harmonic oscillator corresponding to the simulations in figure 3.1 are displayed in figure 3.2.

⁴Another measurement-free preparation protocol for GKP states is described in [29].

4 Oscillator Noise Model

We introduced the stabilization of the GKP code space in chapter 3 as a method to increase the lifetime of information encoded in a GKP state. However, the simulations of the error correction protocol in chapter 3 did not include oscillator or ancilla errors. We now include different sources of noise in the simulations to understand their impact on the lifetime of the logical information encoded in a GKP state. Using this noise model, we also gauge the increase in logical lifetime due to quantum error correction.

For the harmonic oscillator, we consider three Markovian noise channels described by the following Lindblad operators [20]:

1. Single excitation loss: $\sqrt{\gamma_{\text{loss}}(\bar{n} + 1)} \hat{a} \approx \sqrt{\gamma_{\text{loss}}\bar{n}} \hat{a} \equiv \sqrt{\Gamma_{\text{loss}}} \hat{a}$
2. Heating: $\sqrt{\gamma_{\text{loss}}\bar{n}} \hat{a}^\dagger \equiv \sqrt{\Gamma_{\text{loss}}} \hat{a}^\dagger$
3. Dephasing: $\sqrt{\Gamma_\phi} \hat{a}^\dagger a$.

We assume the oscillator to be weakly coupled to a hot bath such that $\bar{n} \approx \bar{n} + 1$ is a good approximation for the average population \bar{n} of the hot bath. This approximation yields an identical loss and heating rate $\Gamma_{\text{loss}} \equiv \gamma_{\text{loss}}\bar{n}$. The parameter Γ_ϕ defines the rate at which the dephasing Lindblad operator is applied to the state of the oscillator.

Furthermore, we include a coherent oscillation of the harmonic oscillator frequency with an amplitude $2\pi\chi$ and frequency¹ ν such that the Hamiltonian of the system in the frame rotating with the average harmonic oscillator frequency yields

$$\hat{H}(t) = 2\pi\chi \sin(2\pi\nu t + \phi) \hat{a}^\dagger a \quad (4.1)$$

with ϕ a constant phase. The phase ϕ is not measured during the experiment and therefore traced out in the performed simulations employing a quantum Monte Carlo simulation with a random $\phi \in [0, 2\pi)$ for every trajectory.

In the subsequent simulations, the error correction protocol is considered as an instantaneous and noise-free oscillator-ancilla circuit. Therefore, ancilla errors are not considered. Also potential preparation errors of the ancilla qubit in the $|+\rangle$ state are neglected. Overall, the time

¹The units of ν and χ are Hz such that $2\pi\nu$ and $2\pi\chi$ are angular frequencies.

Table 4.1: Experimental parameters relevant for simulations. The Δ parameter is obtained from fitting a Gaussian envelope to the experimentally obtained Wigner function of a GKP state. The parameter ξ is the squeezing parameter of the initial state of the oscillator and is optimized for ideal state preparation using the stabilization protocol. δt denotes the time it takes to apply the stabilization circuit to one quadrature. Obtained by adding respective pulse lengths. Accordingly, $2 \times \delta t$ is the time one full error correction cycle takes. The parameters ν and χ are introduced in eq. 4.1 and measured with line-triggered spectroscopy of the RSB varying drive frequency and wait time. [cf. Luise Müller’s semester project report] Γ_{loss} is also measured employing RSB spectroscopy. Γ_ϕ is optimized such that simulations fit experimental data (see discussion below).

Parameter	Value
Δ	0.37
ξ	0.52
$2 \times \delta t$	$2 \times 44.48 \mu\text{s}$
ν	50 Hz
χ	150 Hz
Γ_{loss}	7 q/s
Γ_ϕ	$2\pi \times 27 \text{ Hz}$

evolution of the system without stabilization is described by the master equation

$$\dot{\rho} = -i[\hat{H}(t), \rho] + \Gamma_{\text{loss}}\mathcal{D}[\hat{a}](\rho) + \Gamma_{\text{loss}}\mathcal{D}[\hat{a}^\dagger](\rho) + \Gamma_\phi\mathcal{D}[\hat{a}^\dagger a](\rho) \quad (4.2)$$

with $\mathcal{D}\bullet$ the dissipator introduced in chapter 3. Error correction cycles are included in the simulations by first evolving the state by a time δt (cf. eq. 4.2), applying the stabilization circuit eq. 3.6 on the final state of that time evolution, and using the resulting state as the initial state for the subsequent time evolution by another time δt (cf. eq. 4.2). This procedure is repeated for a given number of error correction rounds. Here, δt denotes the time needed

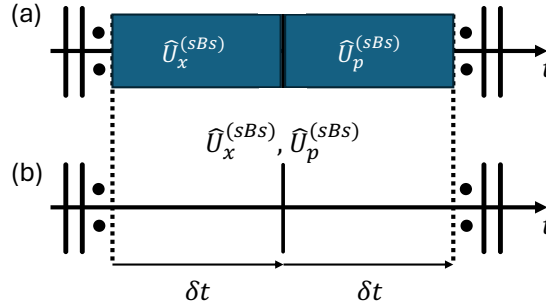


Figure 4.1: Schematic illustration of stabilization protocol. **(a)** Experimental situation. Stabilization of each quadrature takes time δt . **(b)** Simulated stabilization protocol. Time evolution by δt (cf. eq. 4.2), instantaneous stabilization of both quadratures, and subsequent time evolution again by δt (cf. eq. 4.2).

4 Oscillator Noise Model

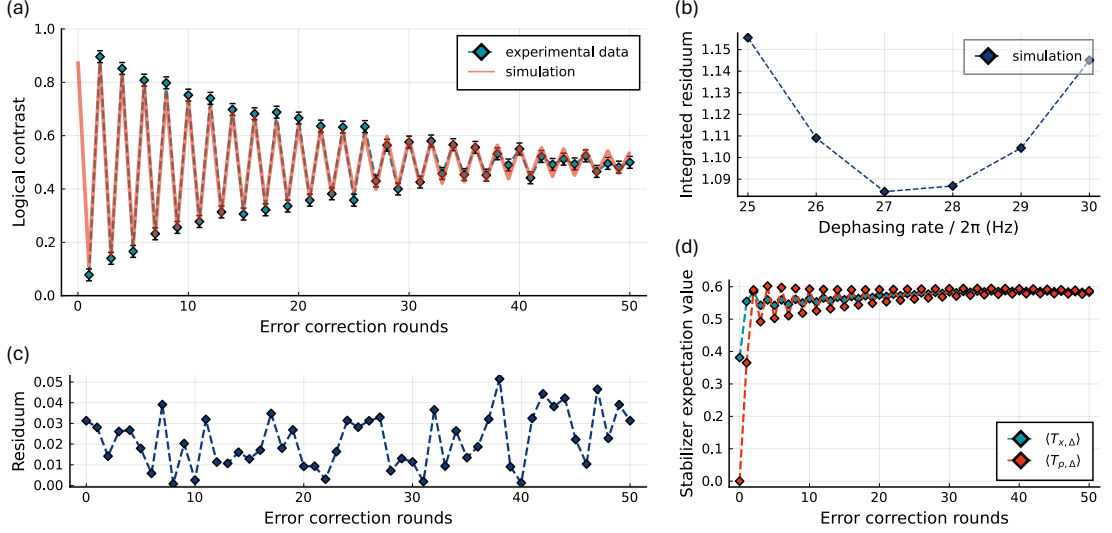


Figure 4.2: Connecting the noise model to the experiment by finding the dephasing rate Γ_ϕ . Utilized experimental parameters are summarized in table 4.1. GKP states are simulated for $x \in [-7.5\sqrt{\pi}, 7.5\sqrt{\pi}]$ with 150 discretization points. Averaged over 15 trajectories to trace out the random phase ϕ . **(a)** Logical contrast $C_L = (1 + \langle \hat{Z}_0 \rangle)/2$ as a function of the number of error correction rounds. Measurement performed with 500 shots per data point. Error bars of experimental data according to discussion in [30]. Orange curve represents simulation with optimized dephasing rate Γ_ϕ . **(b)** Optimization of Γ_ϕ . Integrated residuum $\sum |C_{L,\text{measurement}} - C_{L,\text{simulation}}|$ is plotted in dependence on Γ_ϕ . Dephasing rate Γ_ϕ with minimum integrated residuum is chosen (cf. value in table 4.1). **(c)** Residuum $|C_{L,\text{measurement}} - C_{L,\text{simulation}}|$ for optimized dephasing rate Γ_ϕ (cf. value in table 4.1). **(d)** Simulated finite energy stabilizer expectation value in dependence on number of performed error correction rounds. Note that (d) cannot be directly compared to figure 3.1 (d) because of a different value for Δ .

for stabilization of one quadrature such that $2 \times \delta t$ is the time needed for one full stabilization cycle. The experimental stabilization procedure and its idealized version for the simulations are visualized schematically in figure 4.1 (a) and (b), respectively. The numerical solution of eq. 4.2 is achieved with the master equation solver from the QuantumOptics Julia library. The stabilization circuit is applied numerically according to eq. 3.6 using the CVsim Julia library developed by Ivan Rojkov.

The experimental parameters of the GKP setup at TIQI group relevant for these simulations are summarized in table 4.1. Note how the parameters $\Delta, \xi, \delta t, \nu, \chi$, and Γ_{loss} can be accessed experimentally. The value for Γ_ϕ is optimized such that the noise model accurately fits experimental data: We measure the logical contrast $(1 + \langle \hat{Z}_0 \rangle)/2$ as a function of the number of performed error correction rounds. Note that we perform an infinite energy readout of the

4 Oscillator Noise Model

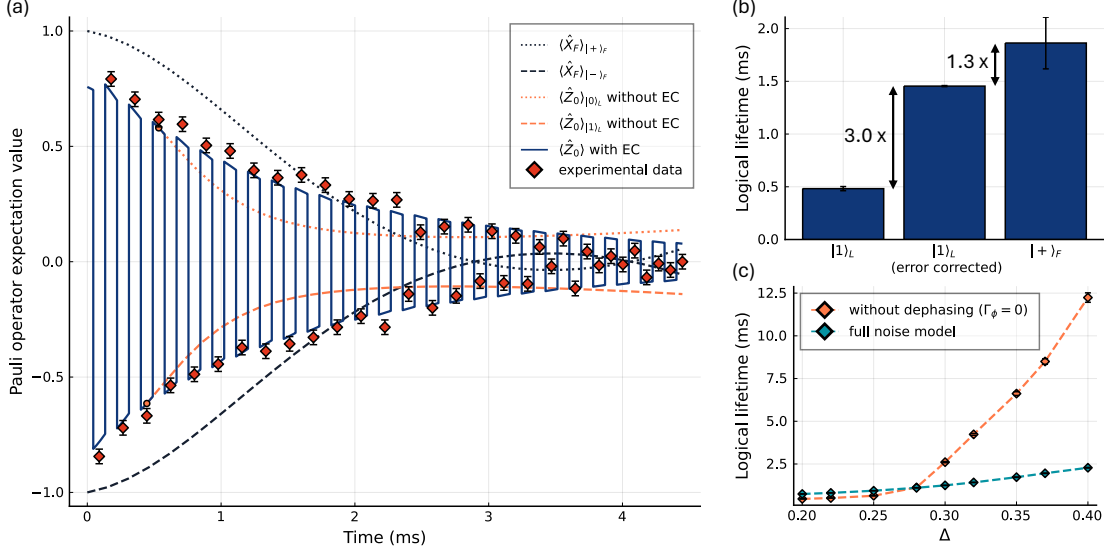


Figure 4.3: Comparing logical lifetimes. GKP states are simulated for $x \in [-7.5\sqrt{\pi}, 7.5\sqrt{\pi}]$ with 150 discretization points. Averaged over 15 trajectories to trace out the random phase ϕ . **(a)** Plot corresponds to figure 4.2 (a) with the time on the x-axis instead of the number of error correction rounds. y-axis shows Pauli operator expectation values instead of logical contrast. Blue curve illustrates simulation of infinite energy Pauli \hat{Z}_0 measurement when simulating error correction with parameters in table 4.1 according to the procedure illustrated in figure 4.1 (b). Blue curve corresponds to orange curve in figure 4.2 (a). Initial state is squeezed vacuum state with $\xi = 0.52$. Red points correspond to measurement points shown in figure 4.2 (a) with error bars again according to [30]. Orange curves indicate infinite energy Pauli \hat{Z}_0 measurement for time evolution due to eq. 4.2 without stabilization and after approximately preparing the $|0\rangle_L$ ($|1\rangle_L$) state by applying 6 (5) sBs stabilization cycles. Black curves show simulation of Pauli $\hat{X}_F = |+\rangle_F \langle +|_F - |-\rangle_F \langle -|_F$ measurement of $|+\rangle_F = (|0\rangle + |1\rangle)/\sqrt{2}$ and $|-\rangle_F = (|0\rangle - |1\rangle)/\sqrt{2}$ Fock states as initial states. The same noise model defined by the parameters listed in table 4.1 is utilized. **(b)** Lifetimes corresponding to orange curve (no QEC), blue curve (with QEC), and black curves (Fock encoding). Obtained by fitting an exponential decay to the respective simulations in (a). Error bars due to standard errors from fits. Simulated logical lifetimes are 0.482 ± 0.020 ms, 1.455 ± 0.006 ms, and 1.86 ± 0.25 ms for $|1\rangle_L$, $|1\rangle_L$ (EC), and $|+\rangle_F$, respectively. **(c)** Logical lifetime depending on the size of the GKP state. Lifetimes again obtained by fitting an exponential decay to simulation of infinite energy Pauli \hat{Z}_0 measurement and error bars again due to standard errors from fits. Initial state of simulations is squeezed vacuum state with $\xi = 0.52$. Turquoise curve shows simulation results for full noise model. Orange curve shows simulation results for identical noise model except for $\Gamma_\phi = 0$.

GKP state.² The measured data is plotted in turquoise color in figure 4.2 (a). The simulation

²The conditional displacement operation also allows for readout of the characteristic function $\chi(\alpha) \equiv \langle \hat{D}(\alpha) \rangle$ with $\hat{D}(\alpha) = e^{\alpha \hat{a}^\dagger - \alpha^* \hat{a}}$ the displacement operator. [31] With $\hat{Z}_0 = e^{i\sqrt{\pi}\hat{x}} = e^{i\sqrt{\pi/2}(\hat{a} + \hat{a}^\dagger)} = \hat{D}(i\sqrt{\pi/2})$ (cf. chapter 2), a Pauli \hat{Z}_0 operator measurement can be obtained from a characteristic function measurement at $\alpha = i\sqrt{\pi/2}$, i.e., $\langle \hat{Z}_0 \rangle = \chi(i\sqrt{\pi/2})$.

4 Oscillator Noise Model

corresponding to this experiment (cf. figure 4.3 (a)) is carried out by following the procedure visualized in figure 4.1 (b) with the parameters summarized in table 4.1. Note that we trace out the random phase ϕ using a quantum Monte Carlo simulation. The only free parameter of the noise model Γ_ϕ is optimized for a minimum integrated residuum comparing the simulation and experimental data (cf. figure 4.2 (a), (b), and (c)). This yields the value for Γ_ϕ in table 4.1. Figure 4.2 (d) shows how the simulated finite energy stabilizer expectation values reach a steady state at $\langle \hat{T}_{x,\Delta} \rangle \approx \langle \hat{T}_{p,\Delta} \rangle \approx 0.6$ for the parameters in table 4.1.

The noise model introduced above can now be utilized to further simulate how the logical lifetime compares with versus without error correction and to different encodings other than the GKP code, e.g., the Fock encoding. This is illustrated in figure 4.3 (a). Fitting an exponential to the time evolution of the Pauli operator expectation values yields the respective logical coherence times of the stored information. The resulting lifetimes are indicated in figure 4.3 (b). We observe a logical lifetime improvement of a factor of 3.0 when comparing the lifetime of a logical GKP state with versus without error correction.

The simulation result for the lifetime of the $|+\rangle_F$ Fock state does *not* match the experimentally observed lifetime of a Fock state of 5 – 10 ms. This indicates that the found dephasing rate Γ_ϕ is overestimated. This is likely due to neglecting errors of the ancilla and errors during the stabilization circuit. We proceed with simulations utilizing the values summarized in table 4.1 but note that an accurate description of the experiment would require a more complete noise model. However, the methods presented hereafter are easily transferred to a more general noise model.

Another parameter that might be of interest given a noise model of the system, is the size of the GKP states defined by Δ . In figure 4.3 (c), we show how the logical lifetime of a GKP state depends on Δ . We observe that for decreasing Δ , i.e., a larger or higher-energy GKP state, the lifetime decreases. For the GKP state size in the experiment $\Delta = 0.37$, the lifetime seems to be mostly limited by dephasing noise. This can be seen by comparing the turquoise and orange curve in figure 4.3 (c) at $\Delta = 0.37$. However, for small Δ , the contribution of other noise sources, such as coherent noise or single excitation loss/heating seems to dominate.

5 Noise Error Budget Simulation

The noise model introduced in chapter 4 is fully defined by the four parameters $\nu, \chi, \Gamma_{\text{loss}}$, and Γ_{ϕ} . In the scope of this chapter, we assume a fixed coherent noise frequency of $\nu = 50$ Hz such that three noise parameters remain. This assumption is reasonable because the power line is identified as the origin of the noise observed in the experiment. As we have seen in chapter 4, the introduced noise model allows for simulations of the time evolution of a given initial state both with and without error correction. Simulating the time evolution of the state of the system allowed us to, e.g., extract the time evolution of the Pauli operator expectation value $\langle \hat{Z}_0 \rangle$. The resulting time trace yields an approximately exponentially decaying curve that can be fitted to obtain the logical lifetime $1/\Gamma_{\text{tot}}$ with Γ_{tot} the decay rate of the Pauli \hat{Z}_0 measurement (cf. figure 4.3 (a) and (b)).

In this chapter, we will explore how we can access the noise error budget of the stabilization protocol, i.e., simulate how improvements in the respective error rates would translate to a logical lifetime improvement. In particular, such a noise error budget simulation can provide insight into the relative contribution of different noise channels toward the decoherence of the stored logical information. This noise error budget simulation requires a model that relates the noise parameters $\Gamma_{\text{loss}}, \Gamma_{\phi}$, and χ to the logical decoherence rate Γ_{tot} . For small changes in the noise parameters in the vicinity of the parameters of the experiment (cf. table 4.1), we can justify a linear model

$$\Gamma_{\text{tot}} = A\Gamma_{\text{loss}} + B\Gamma_{\phi} + C\chi + \text{cst.}, \quad (5.1)$$

with free parameters A, B, C , and an offset constant.¹ We can now proceed to simulate the decoherence rate Γ_{tot} for noise parameters $\Gamma_{\text{loss}}, \Gamma_{\phi}$ and χ that lie in the vicinity of the error parameters found for the experiment. We fix the other parameters defining the simulations to the values listed in table 4.1. The generated data points $(\Gamma_{\text{tot}}; \Gamma_{\text{loss}}, \Gamma_{\phi}, \chi)$ can then be fitted

¹A function f that aims to describe how the logical decoherence rate Γ_{tot} is related to the noise parameters $\Gamma_{\text{loss}}, \Gamma_{\phi}$, and χ , i.e., $\Gamma_{\text{tot}} = f(\Gamma_{\text{loss}}, \Gamma_{\phi}, \chi)$, should asymptotically fulfill $f(0, 0, 0) \rightarrow 0$ since we expect an increasing lifetime (decreasing decoherence rate) of the GKP state with fewer noise sources present, i.e., for smaller coupling to the environment. However, this is only true if the function f describes the logical decoherence time for all possible values of $(\Gamma_{\text{loss}}, \Gamma_{\phi}, \chi)$. Eq. 5.1 only aims to linearly approximate the function f close to the noise parameters found for the experiment and can, therefore, exhibit a non-zero offset constant. A non-zero offset constant in eq. 5.1 indicates a non-linear function f and, therefore, validity of eq. 5.1 only in the vicinity of the experimental noise parameters.

5 Noise Error Budget Simulation

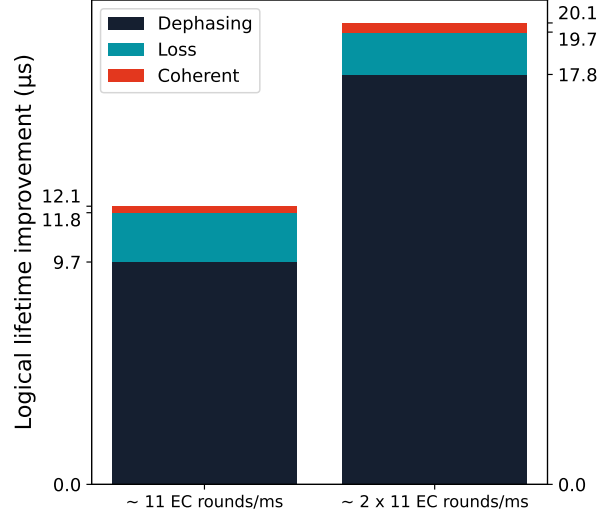


Figure 5.1: Noise error budget. Logical lifetime improvement $\Delta(1/\Gamma_{\text{tot}})$ due to eq. 5.2 given a 1% improvement of the error parameters present in the experiment (i.e., $\Delta\Gamma_{\text{loss}} = 0.01 \times \Gamma_{\text{loss}}$ etc.). GKP states are simulated for $x \in [-5.5\sqrt{\pi}, 5.5\sqrt{\pi}]$ with 150 discretization points. Averaged over 15 trajectories to trace out the random phase ϕ . Simulation procedure: Initial state $|1\rangle_L$ is approximately prepared by applying 5 EC rounds with parameters in table 4.1, where $2 \times \delta t = 2 \times 44.48 \mu\text{s}$ (left) and $2 \times \delta t = 44.48 \mu\text{s}$ (right). Error correction rate is computed with $1/(2\delta t)$. After state preparation, state evolution is continued with modified error parameters $(\Gamma_{\text{loss}}, \Gamma_{\phi}, \chi) \in \{5 \text{ q/s}, 7 \text{ q/s}, 9 \text{ q/s}\} \times \{2\pi \times 26 \text{ Hz}, 2\pi \times 27 \text{ Hz}, 2\pi \times 28 \text{ Hz}\} \times \{140 \text{ Hz}, 150 \text{ Hz}, 160 \text{ Hz}\}$. Time traces of Pauli \hat{Z}_0 measurements are computed and fitted to find corresponding decoherence rates Γ_{tot} . The resulting data points $(\Gamma_{\text{tot}}; \Gamma_{\text{loss}}, \Gamma_{\phi}, \chi)$ are used to fit a linear model according to eq. 5.1 to predict the logical lifetime improvement.

with eq. 5.1 which yields the free parameters A, B, C , and the offset constant.

From the fitted model eq. 5.1, we can now predict the change in logical lifetime $\Delta(1/\Gamma_{\text{tot}})$ given a change of one of the noise parameters $\Delta\Gamma_{\text{loss}}, \Delta\Gamma_{\phi}$, or $\Delta\chi$ by computing

$$\Delta\left(\frac{1}{\Gamma_{\text{tot}}}\right) = \frac{A}{\Gamma_{\text{tot}}^2} \bigg|_{\text{exp. parameters}} \Delta\Gamma_{\text{loss}} \quad (5.2)$$

$$\Delta\left(\frac{1}{\Gamma_{\text{tot}}}\right) = \frac{B}{\Gamma_{\text{tot}}^2} \bigg|_{\text{exp. parameters}} \Delta\Gamma_{\phi} \quad (5.3)$$

$$\Delta\left(\frac{1}{\Gamma_{\text{tot}}}\right) = \frac{C}{\Gamma_{\text{tot}}^2} \bigg|_{\text{exp. parameters}} \Delta\chi. \quad (5.4)$$

The resulting increase of the logical lifetime given a 1% improvement of the noise parameters relative to their value found for the experimental setup (cf. table 4.1) is plotted in figure 5.1 for two different rates of error correction. Clearly, the decoherence of the GKP state is dominantly governed by dephasing noise. The simulations suggest for an error correction rate of $1/(2\delta t) \approx$

5 Noise Error Budget Simulation

11 EC rounds/ms (for the value for $2 \times \delta t$ in table 4.1) that improving the dephasing rate by 1% of its value in the experiment, i.e., $\Delta\Gamma_\phi \approx -2\pi \times 0.27$ Hz, would yield a logical lifetime improvement of $\Delta\Gamma_\phi \approx 9.7$ μ s. Improving the loss rate Γ_{loss} by 1% of its experimental value instead, i.e., $\Delta\Gamma_{\text{loss}} = -0.07$ q/s, would yield $\Delta(1/\Gamma_{\text{tot}}) \approx 2.1$ μ s. Improving the coherent noise amplitude present in the harmonic oscillator appears to only have a little effect on the logical lifetime. Overall, dephasing noise appears to dominate constituting 80% (89%) of the possible lifetime improvement for 11 (22) EC rounds/ms.

The introduced method to compute the noise error budget indicates how different error channels contribute towards the decoherence of logical information stored in a GKP state. Identifying the most dominant error sources by employing this method hints at noise sources that should be improved in the experiment. However, the significance of the computed logical lifetime improvements crucially depends on the accuracy of the underlying noise model. In particular, the influence of ancilla noise on the error budget calculations should be considered with a more elaborate noise model.

6 Conclusion and Outlook

In this semester project report, an oscillator noise model is introduced that includes Markovian oscillator noise, namely single excitation loss, heating, and dephasing, as well as coherent oscillator noise, to describe the decoherence of a stabilized GKP state prepared in the motional degree of freedom of a trapped ion. The error parameters defining the noise model are determined with experiments involving spectroscopy of the red sideband and by optimizing error parameters such that simulations accurately resemble experimental data. Simulations of the stabilization of GKP states using this noise model show error correction to improve the logical lifetime of the GKP states from 0.48(2) ms to 1.45(5) ms. By approximating the total decoherence rate of a GKP state to depend linearly on the noise parameters in the vicinity of the parameters found for the current state of the experiment, a method is introduced to compute the noise error budget for quantum error correction. This method analyzes how improvements in the respective error rates of the noise model would translate to a logical lifetime improvement of the GKP state. The introduced noise model suggests dephasing as the dominant noise source, contributing approximately 80% towards the decoherence of a stabilized GKP state. However, the true contribution of dephasing noise can only be accurately estimated by additionally considering ancilla errors in a future more complete noise model.

In principle, the performed noise error budget calculation suggests which noise sources to improve to achieve a maximum gain in coherence time. However, this requires the noise model to accurately describe the noise sources present in the experiment. The simulated lifetime of 1.8(6) ms for a $|+\rangle_F$ Fock state using the introduced noise model shows a significant deviation from the experimentally observed Fock state lifetime, which lies between 5 and 10 ms. This inconsistent simulation result indicates an overestimation of the dephasing rate, likely due to the assumption of instantaneous noise-free stabilization circuits, specifically neglecting errors occurring in the ancilla qubit. Overall, this observation calls for a more elaborate noise model that also includes errors during the stabilization circuit. Given such a noise model, the method to compute the noise error budget introduced in chapter 5 can be employed in an identical manner by including other error parameters into the linear model. However, note that simulating data points (Γ_{tot} ; *err. param. 1*, *err. param. 2*, *err. param. 3*, ...) to fit the linear model (cf. chapter 5) becomes exponentially more expensive as the number of noise model parameters increases

6 *Conclusion and Outlook*

while also becoming less expressive as different noise channels can have similar effects on the GKP state decay.

Bibliography

- [1] Preskill, J. Quantum Computing in the NISQ era and beyond. *Quantum* **2**, 79 (2018).
- [2] Bluvstein, D. *et al.* Logical quantum processor based on reconfigurable atom arrays. *Nature* **626**, 58–65 (2024).
- [3] DiVincenzo, D. P. The Physical Implementation of Quantum Computation. *Fortschritte der Physik* **48**, 771–783 (2000).
- [4] Shor, P. W. Fault-tolerant quantum computation. In *Proceedings of 37th conference on foundations of computer science*, 56–65 (IEEE, 1996).
- [5] Nielsen, M. A. & Chuang, I. L. *Quantum computation and quantum information*, vol. 2 (Cambridge university press Cambridge, 2001).
- [6] Krinner, S. *et al.* Realizing repeated quantum error correction in a distance-three surface code. *Nature* **605**, 669–674 (2022).
- [7] Google Quantum AI *et al.* Suppressing quantum errors by scaling a surface code logical qubit. *Nature* **614**, 676–681 (2023).
- [8] De Neeve, B., Nguyen, T.-L., Behrle, T. & Home, J. P. Error correction of a logical grid state qubit by dissipative pumping. *Nature Physics* **18**, 296–300 (2022).
- [9] Campagne-Ibarcq, P. *et al.* Quantum error correction of a qubit encoded in grid states of an oscillator. *Nature* **584**, 368–372 (2020).
- [10] Sivak, V. V. *et al.* Real-time quantum error correction beyond break-even. *Nature* **616**, 50–55 (2023).
- [11] Postler, L. *et al.* Demonstration of fault-tolerant universal quantum gate operations. *Nature* **605**, 675–680 (2022).
- [12] Ebadi, S. *et al.* Quantum optimization of maximum independent set using rydberg atom arrays. *Science* **376**, 1209–1215 (2022).

Bibliography

- [13] Fowler, A. G., Mariantoni, M., Martinis, J. M. & Cleland, A. N. Surface codes: Towards practical large-scale quantum computation. *Phys. Rev. A* **86**, 032324 (2012).
- [14] Landahl, A. J., Anderson, J. T. & Rice, P. R. Fault-tolerant quantum computing with color codes. *arXiv:1108.5738* (2011).
- [15] Horsman, D., Fowler, A. G., Devitt, S. & Van Meter, R. Surface code quantum computing by lattice surgery. *New Journal of Physics* **14**, 123011 (2012).
- [16] Vasmer, M. & Browne, D. E. Three-dimensional surface codes: Transversal gates and fault-tolerant architectures. *Physical Review A* **100**, 012312 (2019).
- [17] Brown, B. J. A fault-tolerant non-clifford gate for the surface code in two dimensions. *Science Advances* **6**, eaay4929 (2020).
- [18] Bravyi, S. *et al.* High-threshold and low-overhead fault-tolerant quantum memory. *Nature* **627**, 778–782 (2024).
- [19] Gottesman, D., Kitaev, A. & Preskill, J. Encoding a qubit in an oscillator. *Physical Review A* **64**, 012310 (2001).
- [20] Royer, B., Singh, S. & Girvin, S. Stabilization of Finite-Energy Gottesman-Kitaev-Preskill States. *Physical Review Letters* **125**, 260509 (2020).
- [21] Flühmann, C. *et al.* Encoding a qubit in a trapped-ion mechanical oscillator. *Nature* **566**, 513–517 (2019).
- [22] Flühmann, C. *Encoding a qubit in the motion of a trapped ion using superpositions of displaced squeezed states*. Doctoral thesis, ETH Zürich (2019).
- [23] Rojkov, I. *et al.* Two-qubit operations for finite-energy Gottesman-Kitaev-Preskill encodings (2023). ArXiv:2305.05262 [quant-ph].
- [24] Shaw, M. H., Doherty, A. C. & Grimsmo, A. L. Logical Gates and Read-Out of Superconducting Gottesman-Kitaev-Preskill Qubits (2024). ArXiv:2403.02396 [quant-ph].
- [25] Hahn, O., Ferrini, G. & Takagi, R. Bridging magic and non-Gaussian resources via Gottesman-Kitaev-Preskill encoding (2024). ArXiv:2406.06418 [quant-ph].
- [26] Wang, Z. & Jiang, L. Passive environment-assisted quantum transduction with GKP states (2024). ArXiv:2401.16781 [quant-ph].
- [27] Pantaleoni, G., Baragiola, B. Q. & Menicucci, N. C. Modular Bosonic Subsystem Codes. *Physical Review Letters* **125**, 040501 (2020).

- [28] Haroche, S. & Raimond, J.-M. *Exploring the Quantum* (Oxford University Press, 2006).
- [29] Hastrup, J., Park, K., Brask, J. B., Filip, R. & Andersen, U. L. Measurement-free preparation of grid states. *npj Quantum Information* **7**, 17 (2021).
- [30] Timme, H. *Single-ion addressing using crossed acousto-optic deflectors*. Master thesis, ETH Zürich (2019).
- [31] Flühmann, C. & Home, J. Direct Characteristic-Function Tomography of Quantum States of the Trapped-Ion Motional Oscillator. *Physical Review Letters* **125**, 043602 (2020).